*Article*

# Giant Enhancement of Magnetostrictive Response in Directionally-Solidified $Fe_{83}Ga_{17}Er_x$ Compounds

**Radhika Barua [1,\*], Parisa Taheri [1], Yajie Chen [1], Anjela Koblischka-Veneva [2] ,**
**Michael R. Koblischka [2], Liping Jiang [3] and Vincent G. Harris [1,\*]**

[1]  College of Engineering, Northeastern University, Boston, MA 02115, USA; paris.t14@gmail.com (P.T.);
     y.chen@neu.edu (Y.C.)
[2]  Institute of Experimental Physics, Saarland University, 66123 Saarbrucken, Germany;
     a.koblischka@gmail.com (A.K.-V); m.koblischka@mx.uni-saarland.de (M.R.K.)
[3]  Baotou Research Institute of Rare Earths, Baotou 014010 China; btjlp@126.com
[\*]  Correspondence: radhika.barua@gmail.com (R.B.); harris@ece.neu.edu or vincegharris@gmail.com (V.G.H.)

**Abstract:** We report, for the first time, correlations between crystal structure, microstructure and magnetofunctional response in directionally solidified [110]-textured $Fe_{83}Ga_{17}Er_x$ ($0 < x < 1.2$) alloys. The morphology of the doped samples consists of columnar grains, mainly composed of a matrix phase and precipitates of a secondary phase deposited along the grain boundary region. An enhancement of more than ~275% from ~45 to 170 ppm is observed in the saturation magnetostriction value ($\lambda_s$) of $Fe_{83}Ga_{17}Er_x$ alloys with the introduction of small amounts of Er. Moreover, it was noted that the low field derivative of magnetostriction with respect to an applied magnetic field (*i.e.*, $d\lambda_s/dH_{app}$ for $H_{app}$ up to 1000 Oe) increases by ~230% with Er doping ($d\lambda_s/dH_{app,FeGa} = 0.045$ ppm/Oe; $d\lambda_s/dH_{app,FeGaEr} = 0.15$ ppm/Oe). The enhanced magnetostrictive response of the $Fe_{83}Ga_{17}Er_x$ alloys is ascribed to an amalgamation of microstructural and electronic factors, namely: (i) improved grain orientation and local strain effects due to deposition of Er in the intergranular region; and (ii) strong local magnetocrystalline anisotropy, due to the highly anisotropic localized nature of the *4f* electronic charge distribution of the Er atom. Overall, this work provides guidelines for further improving galfenol-based materials systems for diverse applications in the power and energy sector.

**Keywords:** iron-gallium; magnetostriction; rare-earth doped FeGa

## 1. Introduction

Functional materials systems that demonstrate large magnetostriction play an important role in a wide array of commercial applications, ranging from acoustic sensors and linear actuators to electromechanical energy harvesters and sonar transducers [1–3]. One of the most successful magnetostrictive materials hitherto is the rare-earth compound, $(Dy_{0.7}Tb_{0.3})Fe_2$ (also known as Terfenol D) [4]. These alloys demonstrate a cubic C15 laves crystal structure and exhibit large room temperature magnetic-field-induced strains up to 2000 ppm [4]. It is well known that Terfenol D has several major drawbacks that constrain its use in commercial devices, particularly: (i) high cost and global shortage of the rare-earth elements, Tb and Dy [5]; (ii) low mechanical integrity (high brittleness, low yield stress, low magneto-mechanical coupling) [6]; and (iii) high fields required for magnetic saturation [7]. To this end, a promising alternative to $(Dy_{0.7}Tb_{0.3})Fe_2$ is the rare-earth-free, inexpensive and corrosion resistant $Fe_{1-x}Ga_x$ alloy (commercially known as Galfenol), which exhibits moderate magnetostriction (up to approximately 400 ppm) under a very low magnetic field of 100 Oe and a high tensile strength of 500 MPa in the temperature range from $-20$ to $80\ ^\circ C$ [8].

An intriguing characteristic of $Fe_{1-x}Ga_x$ is that its functional response is closely correlated with its microstructural and crystallographic properties [8]. The binary phase diagram of $Fe_{1-x}Ga_x$ indicates that the single-phase terminal solid solution possesses a chemically disordered body-centered cubic (bcc) crystal structure that extends to Ga concentrations of 11 at.% at room temperature and to as much as 35 at.% Ga at 1050 °C [9]. In the composition range (~27–28 at.% Ga), the alloy also exists as $Fe_3Ga$, and it exhibits a chemically-ordered cubic $L1_2$ crystal structure that undergoes polymorphic transformations to the ordered hexagonal $D0_{19}$ and cubic $D0_3$ phase upon heating [10,11]. Further, a B2 ordered cubic phase variant is also noted at high temperatures for compositions exceeding 32 at.% Ga [10]. Depending upon the sample synthesis and the processing technique employed, significant amounts of Ga (well in excess of the solubility limit) can be retained in a metastable disordered bcc solid solution at room temperature [8,10,12]. High magnetostriction values ranging from 250 to 400 ppm have been reported in single crystals of bcc alloys of $Fe_{1-x}Ga_{x,}$, where $x$ ranges from 15 to 25 [13].

Over the last twenty years, attempts have been made to improve the magnetostrictive response of galfenol by addition of a wide variety of elements into its crystal lattice. In almost all cases, ternary additions of *3d* and *4d* transition metals (V, Cr, Mn, Co, Ni, Rh and Mo) decrease the magnetostriction values, relative to that of the parent binary FeGa alloy [14–18]. While tiny amounts of small interstitial atoms (C, B or N) have a slight but favorable effect on the magnetostriction of FeGa (particularly at high atomic compositions of Ga) [18,19]. More recent studies indicate that the magnetostriction of this compound can be significantly increased by adding small amounts of rare-earth elements ranging from La to Lu [20–28]. A phenomenological model based on the rare-earth crystal field interaction, proposed by He et al., suggests that the best trace dopants are the light rare earths, Ce and Pr (up to 0.2 at.% doping), which give a transverse magnetostriction of up to 800 ppm [24]. However, to date, very little attention has been given to Er-doped FeGa compounds.

To add to the FeGa literature, here, we present, for the first time, an experimental study that aims at investigating the crystallographic, microstructural, magnetic and magnetostrictive properties of a series of Er-doped polycrystalline alloys of composition, $Fe_{83}Ga_{17}Er_x$ ($0 < x < 1.2$). Results obtained in this research effort represent an exceptional increase (~275%) in the magnetostriction coefficient of [110]-textured FeGa alloys. The optimal composition for the best magnetostrictive response was found to be $Fe_{83}Ga_{17}Er_x$ ($x = 0.6$). The origin of the enhanced magnetostrictive effect in this materials system is discussed in the context of the microstructure, as well as the electronic structure of samples. Overall, this work provides pathways for enhancing the functional response of FeGa alloys.

## 2. Materials and Methods

Polycrystalline samples of nominal composition $Fe_{83}Ga_{17}Er_x$ ($0 < x < 1.2$) were synthesized from constituent elements of 99.9% purity, using vacuum arc-melting and directional-solidification techniques. The bulk ingots were subsequently placed in an Ar atmosphere and annealed at 900 °C for two hours to obtain the desired phase and microstructure. The arc-melted charges were then sliced into cuboid-shaped slabs (dimensions: 0.01 m × 0.01 m × 0.001 m) using a low-speed diamond saw for characterization of structural, magnetic and magnetostrictive attributes.

Microstructural analysis was carried out on mechanically polished sample slices using an Electron Backscatter Diffractometer, consisting of a JEOL 700F SEM microscope (JEOL, Welwyn Garden City, UK) equipped with a TSL OIM analysis unit (AMETEK, Leicester, UK) and a laboratory $CuK_\alpha$ X-ray diffractometer (Rigaku Ultima III, Wilmington, MA, USA). Bragg peaks obtained from the X-ray diffraction pattern were least-squares fit to a Pseudo-Voigt function to estimate lattice parameters of the $Fe_{83}Ga_{17}Er_x$ alloys [29]. During electron back-scattering diffraction (EBSD) measurements, Kikuchi patterns were generated using an acceleration voltage of 20 kV, and recorded by means of a DigiView camera system (AMETEK, Leicester, UK) at a recording speed of the order of 0.1 s/pattern. Slightly longer time was required for multi-phase analysis. The working distance was 20 mm, and the step-size of the EBSD system was chosen to be 20 nm. More details regarding the measurement procedures may be found in References [30,31]. The results of the EBSD measurements are presented

in the form of maps, the most important of which are the inverse pole figure (IPF) maps that indicate crystallographic orientation of individual foci.

Magnetic characterization was carried out using a vibrating sample magnetometer (Lake Shore, Model 7400, Westerville, OH, USA) in magnetic fields up to $H_{app}$ = ±1.2 T and in the temperature range (300 K ≤ $T$ ≤ 1000 K). The magnetic transition temperature ($T_t$) was determined as the inflection point in the derivative of magnetization ($M$) as a function of temperature ($T$) at an applied magnetic field of $\mu_0 H$ = 1 T. During magnetostriction measurements, the strain gauge was bonded longitudinally to the Galfenol samples in a quarter-bridge configuration to measure the magnetostrictive coefficient along the direction of growth of the samples. A Vishay Micro-measurement P3 strain Indicator was employed to measure the magnetostrictive strain, as the magnetic field was swept from 0 to 1 T at room temperature (~300 K).

## 3. Experimental Results & Discussion

### 3.1. Structural Attributes: Crystallographic and Microstructural Properties

X-ray diffraction data of the $Fe_{83}Ga_{17}Er_x$ alloys, obtained by scanning the sample plane perpendicular to the growth direction, as shown in Figure 1a, indicates the presence of a single phase having the bcc crystal structure for all samples of composition $x < 0.6$ (lattice parameter, $a$ = 2.905 ± 0.005 Å). An additional Bragg peak corresponding to a minor secondary phase is observed at $2\theta$~42°, as Er dopant concentration ($x$) is increased to $x > 0.6$. Overall, all the samples were found to be polycrystalline in character with a preferred orientation along the [110] growth direction—a feature attributed to the thermal gradient imposed by directional solidification. The dependence of relative X-ray intensity of the Bragg planes (110) and (200) with Er content is illustrated in Figure 1b. At all Er doping concentrations, the (110) plane retains dominance. Nonetheless, it is interesting to note that the (200) plane increases in intensity and displays the largest value for $x = 0.6$. It is hypothesized that Er favors occupation of the (200) planes at $x < 0.6$. These results are essential to further understanding the following measurements of magnetostriction as a function of Er content, as will be discussed in subsequent paragraphs.
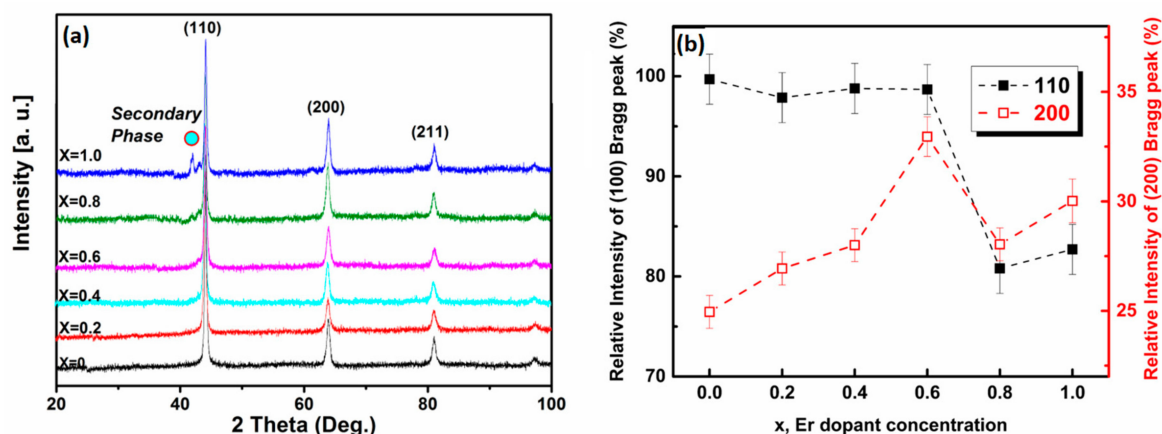


**Figure 1.** (**a**) X-ray diffraction pattern of directional solidified bulk alloys of $Fe_{83}Ga_{17}Er_x$ (0 < $x$ < 1). An additional Bragg peak corresponding to a minor secondary phase is observed in samples where the Er dopant concentration ($x$) is higher than 0.6; (**b**) dependence of the relative intensity of the Bragg peaks corresponding to (110) and (200) planes on Er content ($x$).

The SEM images of select $Fe_{83}Ga_{17}Er_x$ alloys (0 < $x$ < 1) are shown in Figure 2. The microstructure of the parent $Fe_{83}Ga_{17}$ alloy consists of a single solid solution with equiaxed grains of dimensions ~200 μm (Figure 2a). Conversely, the morphology of the Er-doped FeGa alloys demonstrates columnar grains mainly composed of a matrix phase (i.e., gray area) and precipitates of a secondary

phase (i.e., white area) deposited along the grain boundary. The average size of the precipitates was approximately 1–3 µm, and it is observed that the fraction of precipitates increases with Er dopant concentration. Formation of the secondary phase in the $Fe_{83}Ga_{17}Er_x$ alloys is attributed to the realization that the atomic size of Er (175 pm) is significantly larger than that of Fe (140 pm) and Ga (135 pm). This difference in atomic dimensions leads to low solid solubility of Er in the FeGa matrix, and thus, Er exists mostly in the precipitates. This characteristic dual-phase microstructure has been observed previously in other rare-earth doped FeGa alloys [20–22,26,27], and it is considered to be advantageous for improving the magnetostrictive response and mechanical properties of this materials system.
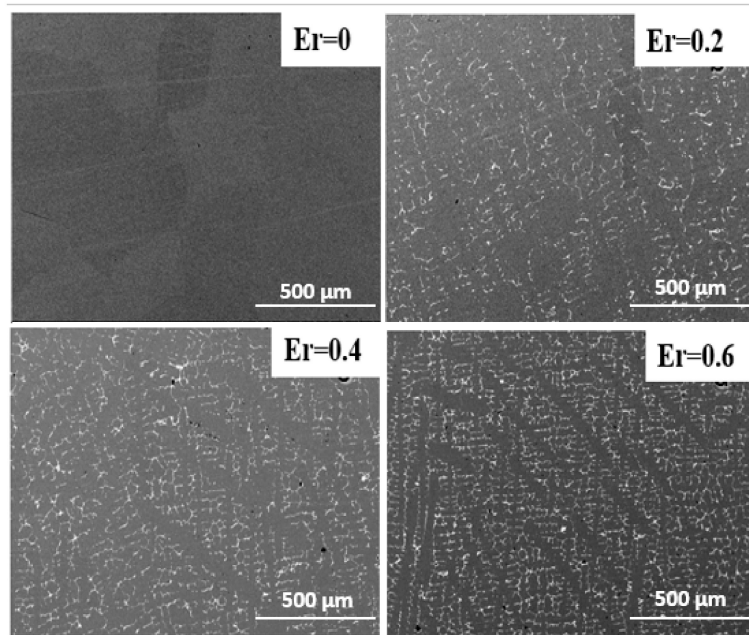


**Figure 2.** A microstructure of Er-doped $(Fe_{0.83}Ga_{0.17})_{100-x}Er_x$ ($x$ = 0, 0.2, 0.4, 0.6).

To determine the distribution of elements, the sample $Fe_{83}Ga_{17}Er_{0.6}$ was analyzed by EDXS. Figure 3 shows SEM morphology and the determination of the constituent elements at spot "a" (grain boundary) and spot "b" (grain). It was found that the grains are composed primarily of Fe and Ga, while the grain boundary consists of Fe and Ga, as well as a relatively high percentage of Er. Stoichiometric determination using EDXS indicates that the Er atoms accumulate more in the grain boundary region and form an intermetallic secondary phase, possibly $Ga_6Er$. Presence of the secondary phase in samples with relatively high Er concentrations is consistent with results obtained by X-ray diffraction analysis (see Figure 1).

Information regarding the texture of the $Fe_{83}Ga_{17}Er_x$ alloys ($0 < x < 1.2$) was obtained using EBSD analysis. Kikuchi patterns obtained using this technique were indexed, using material files pertaining to FeGa (based on bcc $\alpha$-Fe structure; Pearson symbol: cI2) and $Ga_6Er$ (based on tetragonal crystal structure; Pearson Symbol: $tP$14). Here, it should be noted that we could observe the $Ga_6Er$ phase from the sample with $x$ = 0.2. This demonstrates the importance of a highly spatially resolved measurement. Figure 4 shows the IPF maps along the [001] direction (i.e., perpendicular to the sample surface) and corresponding pole figures for the following compositions: $Fe_{83}Ga_{17}$ (i.e., the parent compound), $Fe_{83}Ga_{17}Er_{0.6}$ and $Fe_{83}Ga_{17}Er_{1.2}$. The IPFs shown here provide the crystallographic orientation of the grains, according to the stereographic triangles for each phase. In confirmation with results obtained by X-ray diffraction and SEM-EDS, no $Ga_6Er$ phase was observed in the parent $Fe_{83}Ga_{17}$ compound (Figure 4a). In $Fe_{83}Ga_{17}Er_{0.6}$, the $Ga_6Er$ precipitates were present, as indicated as small spots scattered over the scan area (Figure 4b). Conversely, significant aggregation of $Ga_6Er$

was also found in $Fe_{83}Ga_{17}Er_{1.2}$ (Figure 4c). The IPF maps and the pole figures indicate that while the $Fe_{83}Ga_{17}$ parent compound demonstrates [001] texture, $Fe_{83}Ga_{17}Er_{0.6}$ and $Fe_{83}Ga_{17}Er_{1.2}$ samples do not exhibit preferred grain orientations. It is important to realize that grain size of both the FeGa and the $Ga_6Er$ phases in the $Fe_{83}Ga_{17}Er_x$ samples increased as a function of the Er concentration. As the dopant concentration was increased, $Ga_6Er$ formed a secondary phase in the grain boundary region (Figure 4b,c), and the orientation of the grains is found to be in [001] and [101] directions. When the $Ga_6Er$ is located within the matrix, the grains have the same orientation as the matrix—a feature attributed to the coherent relationship between the two phases. As the grain size of the FeGa and the $Ga_6Er$ phases increases, the crystallographic orientation between these phases became significantly different (see pole figures in Figure 4c), and thus, it is inferred that the secondary phase precipitates were randomly oriented in the matrix phase in the large grained $Fe_{83}Ga_{17}Er_x$ alloys.
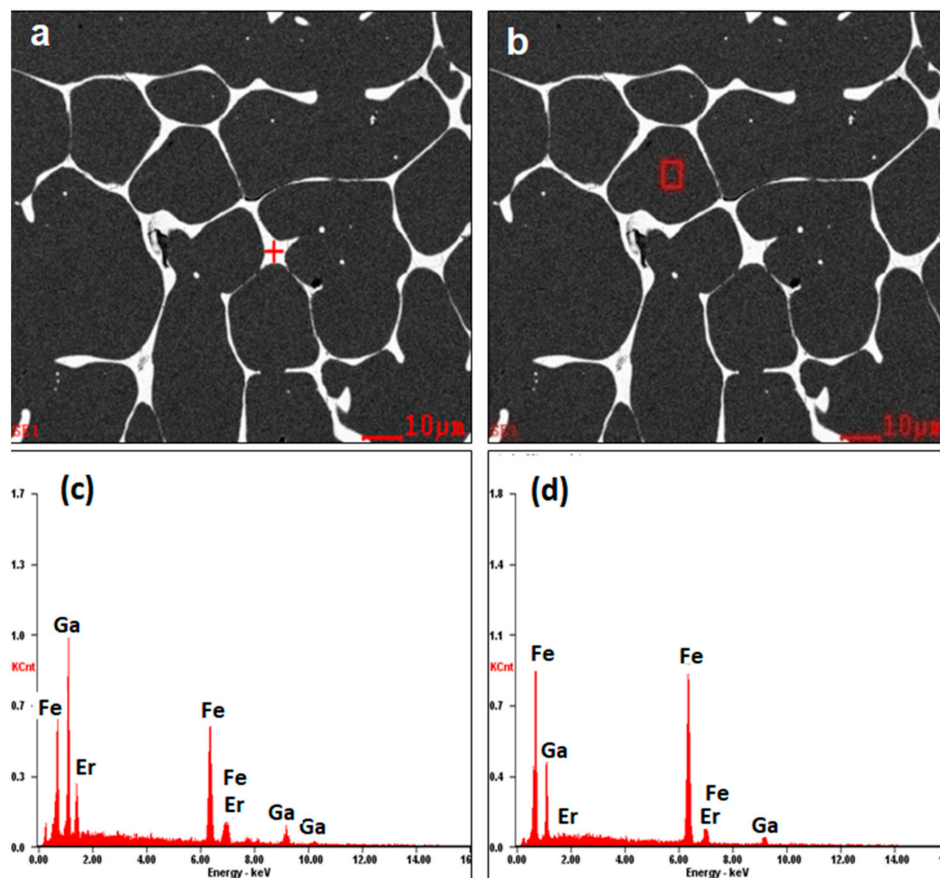


**Figure 3.** (**a**,**b**) SEM morphology of a sample of composition, $Fe_{83}Ga_{17}Er_{0.6}$.; (**c**,**d**) EDXS profile of Fe, Ga and Er in the grain boundary region marked as "+" and in the intragranular region marked as "□".

Addition of Er has noteworthy effects on the magnetic properties of [110]-textured polycrystalline FeGa alloys. The magnetization behavior of $Fe_{83}Ga_{17}Er_x$ alloys ($0 < x < 1.5$) as a function of a magnetic field at room temperature ($T$ = 300 K), shown in Figure 5a, indicates that doping with Er increases the saturation magnetization ($M_s$) by approximately 10%, as compared to the $Fe_{83}Ga_{17}$ parent alloy. As shown in the inset of Figure 5a, $M_s$ initially increases from 153.8 to 168.2 emu/g, as the Er content increased from 0 to 0.6. Further increase in Er doping decreases $M_s$ slightly—a feature attributed to the significant presence of the secondary $Ga_6Er$ phase. The temperature-dependent magnetization behavior of the $Fe_{83}Ga_{17}Er_x$ samples at an applied magnetic field of $H$ = 1000 Oe is shown in Figure 5b. Consistent with previous reports, the Curie temperature of $Fe_{83}Ga_{17}$ was found to

be approximately 990 K [8]. Overall, the $T_c$ of the $Fe_{83}Ga_{17}Er_x$ samples was found to be independent of the Er concentration.
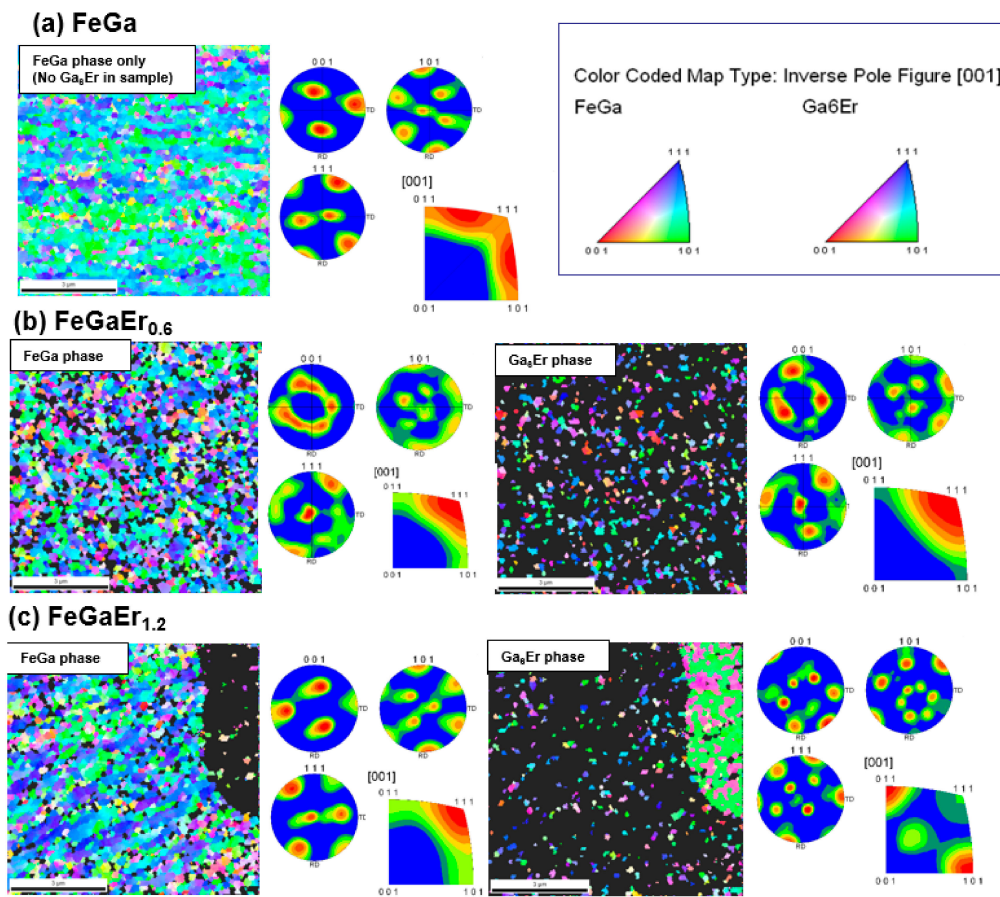


**Figure 4.** Inverse pole figure maps and corresponding pole figures for FeGa and the $Ga_6Er$ phases in samples of the following compositions: (**a**) $Fe_{83}Ga_{17}$ (parent compound); (**b**) $Fe_{83}Ga_{17}Er_{0.6}$ and (**c**) $Fe_{83}Ga_{17}Er_{1.2}$. The inverse pole figures shown here give the crystallographic orientation of the grains, according to the stereographic triangles for each phase.
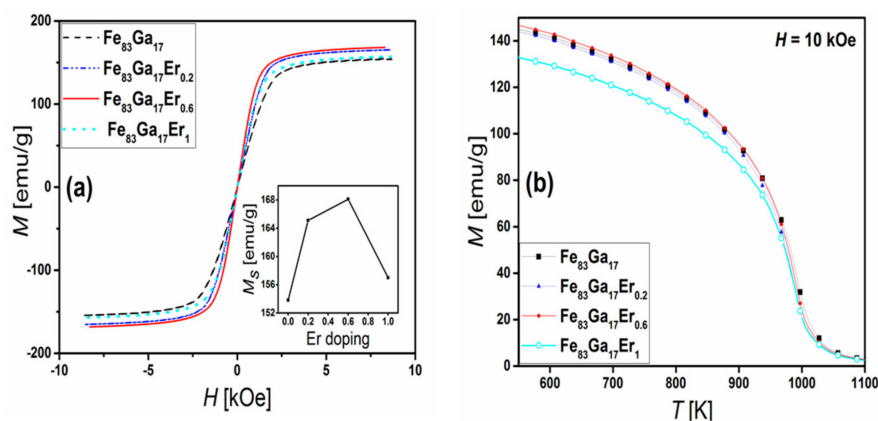


**Figure 5.** (**a**) Magnetization hysteresis loops of $Fe_{83}Ga_{17}Er_x$ ($x = 0, 0.2, 0.6, 1$). The inset shows the saturation moment as a function of the Er doping amount; (**b**) Magnetization (emu/g) of $(Fe_{0.83}Ga_{0.17})_{100-x}Er_x$ at $H = 10$ k Oe as a function of temperature for different amounts of Er doping.

### 3.2. Enhanced Functional Response: Magnetostriction Measurements at Room Temperature

The magnetostriction strain ($\lambda$) along the direction of growth of the $Fe_{83}Ga_{17}Er_x$ alloys is plotted as a function of an applied magnetic field in Figure 6a. In all samples, $\lambda$ increases with applied magnetic field until a saturation magnetostriction value ($\lambda_s$) is obtained. In agreement with previous studies on directionally solidified [110]-textured FeGa alloys [21], the $\lambda_s$ of $Fe_{83}Ga_{17}$ was found to be ~45 ppm. Change in $\lambda_s$ with Er content ($x$) for the $Fe_{83}Ga_{17}Er_x$ alloys is shown in Figure 6b. Overall, $\lambda$ increased with Er doping till the maximum of 170 ppm was achieved at $x = 0.6$. These results represent a record enhancement of more than ~275% in $\lambda_s$ of $Fe_{83}Ga_{17}Er_x$ alloys with the introduction of small amounts of Er. For operation in actuators and sensors in low loss magnetoelectric and multiferroic devices, such as those described in References [32–36], magnetostrictive materials must be operated under mechanical and magnetic bias conditions to achieve the maximum strain per unit magnetic field. Thus, permeability ($\mu$) as realized from the derivative of magnetization/magnetostriction with respect to applied magnetic field ($dM/dH_{app}$ or $d\lambda/dH_{app}$) is a desired figure of merit in magnetostrictive materials. To this end, it is critical to observe from Figure 6a that the low field derivative of magnetostriction with respect to the applied magnetic field ($d\lambda/dH_{app}$ for $H_{app}$ up to 1000 Oe) increases by ~230% with Er doping ($d\lambda_s/dH_{app,FeGa} = 0.045$ ppm/Oe; $d\lambda_s/dH_{app,FeGaEr} = 0.15$ ppm/Oe).
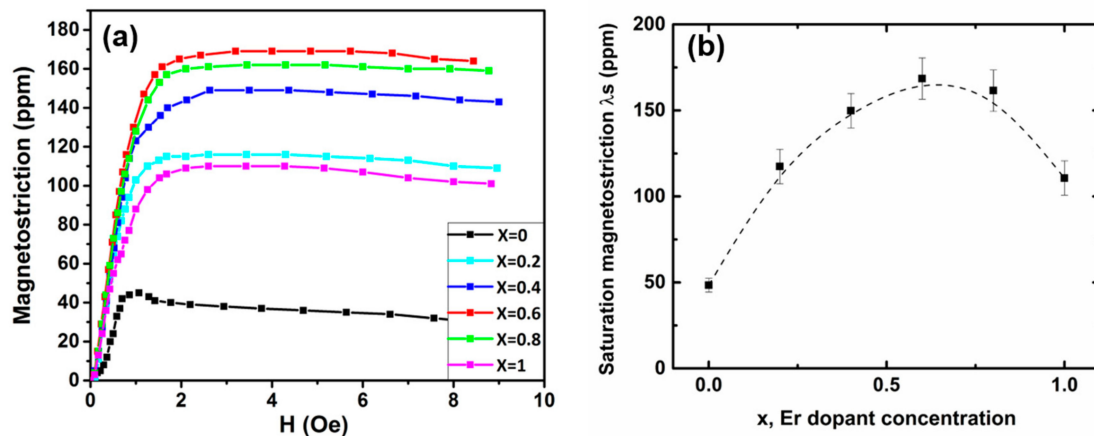


**Figure 6.** (**a**) Magnetostriction of the $(Fe_{0.83}Ga_{0.17})_{100-x}Er_x$ ($0 < x < 1$) alloys as a function of the applied magnetic field. An enhanced saturation magnetostriction value ($\lambda_s$) of more than 250% is measured relative to the parent compound; and (**b**) change in $\lambda_s$ as a function of the Er dopant concentration ($x$).

For FeGa single crystals, a maximum in magnetostriction is reported along the easy magnetic axis, i.e., along the <100> crystallographic direction. Assuming the approximation of only dipole–dipole interactions within the material, the magnetostriction values for a [110]-textured polycrystalline materials may be calculated using the expression [8]:

$$\lambda_{110} = \frac{1}{4}\lambda_{100} + \frac{3}{4}\lambda_{111} \tag{1}$$

where $\lambda_{100}$ and $\lambda_{111}$ are the saturation magnetostriction when the crystal is magnetized and the strain is measured along the <100> and <111> directions, respectively. In the absence of compressive pre-stress, the calculated values of $(3/2)\lambda_{100}$ and $(3/2)\lambda_{111}$ for $Fe_{83}Ga_{17}$ are ~311 ppm and −20 ppm, respectively [37]. Note, that the factor 3/2 arises from the definition of magnetostriction as a deformation from a demagnetized state [37]. The theoretical $(3/2)\lambda_{110}$ value for a polycrystalline $Fe_{83}Ga_{17}$ sample was in approximate agreement with our experimentally determined magnetostriction value of $\lambda_{110} = 45 \pm 5$ ppm. It is critical to note that the use of Equation (1) for the $Fe_{83}Ga_{17}Er_x$ alloys was based on the broad postulation that the texturing degree of the doped samples is similar to that of the pure $Fe_{83}Ga_{17}$ sample.

The $(3/2)\lambda_{110}$ results of [110]-textured rare-earth doped FeGa alloys is summarized in Table 1 with relevant references. It is important to note that with an exception of one report concerning $Fe_{83}Ga_{17}Ce_{0.8}$ [22], the $Fe_{83}Ga_{17}Er_{0.6}$ sample demonstrates higher magnetostriction than any other [110]-textured directionally-solidified FeGa alloy synthesized to date.

**Table 1.** Magnetostriction coefficients of [110]-textured rare-earth doped FeGa alloys synthesized via the directional solidification technique.

| Alloy | Fabrication Technique | $\lambda_{110}$ (ppm) | Condition | References |
|---|---|---|---|---|
| $Fe_{83}Ga_{17}$ | Directional solidification | 45 | Bulk; Pre-stressed | Current work |
| $Fe_{83}Ga_{17}$ | Directional solidification | 68 | Bulk; Pre-stressed | L. Jiang et al. [20] |
| $Fe_{81}Ga_{19}Tb_{0.3}$ | Directional solidification | 85 | Bulk; Pre-stressed | T.I. Fitchorov et al. [34] |
| $Fe_{83}Ga_{17}Y_{0.64}$ | Directional solidification | 133 | Bulk; Compressed under 15 MPa | L. Jiheng et al. [23] |
| $Fe_{83}Ga_{17}Tb_{0.2}$ | Directional solidification | 160 | Bulk; Pre-stressed | L. Jiang et al. [20] |
| $Fe_{83}Ga_{17}Er_{0.6}$ | Directional solidification | 170 | Bulk; Pre-stressed | Current work |
| $Fe_{83}Ga_{17}Ce_{0.8}$ | Directional solidification | 200 | Bulk; Pre-stressed; Sample not at saturation | Z. Yao et al. [22] |

At present, the enhanced magnetostrictive response of the doped $Fe_{83}Ga_{17}Er_x$ alloys is attributed to a combination of electronic and microstructural effects. Previous studies on binary FeGa alloys, conducted by Clark et al., suggest that the large magnetostriction in this intermetallic alloy originates from local magnetocrystalline anisotropy, induced by local short-range interactions between the Ga atoms along specific crystallographic directions in the disordered bcc $\alpha$-Fe structure [37]. It is likely that a large number of *4f* valence electrons and aspherical charge cloud distributions observed in Er atoms lead to enhanced magnetic anisotropy due to crystalline electric field effects. Considering that Er possesses a larger atomic radius (178 pm) relative to Fe (127 pm) and Ga (140 pm), it is possible that the strain due to local lattice distortions influence the magnetic properties of the $Fe_{83}Ga_{17}Er_x$. In related compounds, namely Tb- and Ce-doped directionally solidified FeGa systems, an increase in magnetostriction has been linked to improved grain orientation and morphology [23,24]. Based on experimental and computational studies conducted by He et al., it is surmised that the giant magnetostriction in rare-earth doped FeGa alloys may be ascribed to the presence of nano-heterogeneties in the samples [28]. The dopants tend to enter the nano-heterogeneities, creating a larger tetragonal distortion of the matrix, as well as increased magnetocrystalline anisotropy. A mesoscopic model developed using phase field simulations shows that the bulk tetragonal distortion arises mainly from those nano-heterogeneities with fixed Ga–Ga pairs parallel to the applied magnetic field [28].

It is worth discussing the experimental results obtained in this study in the context of the phenomenological model reported by He et al. to predict magnetostrictive trends in FeGa alloys doped with rare-earth elements [24]. According to this model, the elements (i.e., Ce, Pr and Tb) have the greatest impact on magnetostriction of FeGa among all the rare-earth elements, due to the negative rare-earth quadrupole moment and local lattice tetragonal distortion of the matrix, which is triggered by the heterogeneous nanostructure with local tetragonal distortion [24]. If this were indeed true, the magnetostrictive behavior of the directionally solidified [110]-textured $Fe_{83}Ga_{17}Tb_x$ compounds investigated by Fitchorov et al. [34] and Jiang et al. [20] would be greater than that of the $Fe_{83}Ga_{17}Er_x$ samples examined in the current study. However, our experimental results suggested otherwise. Insight into a potential explanation for this contradiction may be obtained by comparing structure-magnetic property correlations between $Fe_{83}Ga_{17}Er_x$ and $Fe_{83}Ga_{17}Tb_x$ alloys. In both materials systems, only trace amounts of rare-earth dopants were required for optimal magnetostrictive performance in the $Fe_{83}Ga_{17}Er_x$ and $Fe_{83}Ga_{17}Tb_x$ systems. Excessive doping destroys magnetostriction, due to limited solid solubility of the rare-earth element in the FeGa lattice and subsequent formation of the intergranular secondary phases. The maximum magnetostriction in the [110]-textured directionally solidified $Fe_{83}Ga_{17}Er_x$ and related $Fe_{83}Ga_{17}Tb_x$ system was observed at $x = 0.6$ and 0.2 respectively, and thus, it is speculated that the solid solubility of Er in FeGa may be slightly more than that of

Tb. It is further hypothesized that enhancement of magnetostriction may be achieved either by the application of a compressive pre-stress or by increasing the solid solubility of Er in the bcc FeGa matrix through quenching during the cooling phase of the sample fabrication technique. Indeed, previous studies in the FeGa literature demonstrate that the saturation magnetostriction of $Fe_{83}Ga_{17}$ alloys can be remarkably increased by the melt spinning method [22,38]. It is, however, critical to note that it is difficult to experimentally measure the magnetostriction of melt-spun ribbons, as the grains in the sample usually grow perpendicular to the direction of sample growth [22]. Moreover, due to large demagnetizing effects, shape anisotropy in FeGa ribbon samples typically leads to high magnetic saturation fields [38]. From the perspective of user inspired research, the directional solidification technique is more amenable for commercial production of rare-earth doped FeGa alloys.

## 4. Conclusions

In summary, in this work we present the effects of Er additives upon the microstructure, magnetic and microstructural properties of $Fe_{83}Ga_{17}Er_x$ alloys prepared by vacuum arc-melting and directional solidification methods. Data obtained in this experimental study indicate a room temperature magnetostriction value of 170 ppm in a [110]-textured polycrystalline sample of nominal composition $Fe_{83}Ga_{17}Er_{0.6}$—a value that is ~275% higher than that of the corresponding parent $Fe_{83}Ga_{17}$ compound. Overall, addition of small amounts of Er into the FeGa lattice results in an increase in saturation magnetization and magnetostriction and a reduction in the saturation field. These characteristics are beneficial for practical applications, such as actuators in multiferroic magnetic field generators that use a converse magnetoelectric effect or high-sensitivity magnetic field sensors that operate based on the direct magnetoelectric effect without the need for a bias DC field. The enhanced magnetostrictive response of the $Fe_{83}Ga_{17}Er_x$ alloys is ascribed to an amalgamation of electronic and microstructural factors, namely: (i) strong local magnetocrystalline anisotropy due to the large spin-orbit coupling and the highly anisotropic localized nature of the *4f* electronic charge distribution of the Er atom, (ii) improved grain orientation and morphology due to deposition of Er in the intergranular region and (iii) local strain effect that may arise due to incorporation of Er into the FeGa lattice. Excessive Er doping destroys the improved magnetostriction in $Fe_{83}Ga_{17}Er_x$ alloys, due to formation of an undesirable secondary phase, which is identified as the intermetallic compound, $Ga_6Er$. Overall, these results highlight the potential for modifying the functional response of FeGa alloys by addition of tiny amounts of the rare-earth element, Er. To further understand the origin of the superior functional response of rare-earth doped FeGa systems, future work involving computational modeling of the magnetostrictive behavior of these compounds is desired.

**Author Contributions:** R.B. analyzed experimental data, prepared the manuscript and compiled the graphical images, P.T. performed experiments and prepared the initial draft of the manuscript, A.K.-V. And M.R.K. performed EBSD experiments, Y.C. helped design the study, L.J. synthesized the samples used in the study and finally V.G.H. designed the study, helped analyze the data and approved the final manuscript.

**Conflicts of Interest:** The authors declare no conflicts of interest.

## References

1. Parsons, M.J.; Datta, S.; Mudivarthi, C.; Na, S.M.; Flatau, A. Torque sensing using rolled galfenol patches. In Proceedings of the SPIE Smart Sensor Phenomena, Technology, Networks, and Systems, San Diego, CA, USA, 7 April 2008; Volume 6933, p. 693314.
2. Weng, L.; Wang, B.; Dapino, M.J.; Sun, Y.; Wang, L.; Cui, B. Relationships between magnetization and dynamic stress for Galfenol rod alloy and its application in force sensor. *J. Appl. Phys.* **2013**, *113*, 17A917. [CrossRef]

3.   Berbyuk, V. Vibration energy harvesting using Galfenol-based transducer. In Proceedings of the SPIE: Active and Passive Smart Structures and Integrated Systems, San Diego, CA, USA, 10 April 2013; Volume 8688, p. 86881F.

4.   Clark, E.; Teter, J.P.; McMasters, O.D. Magnetostriction "jumps" in twinned $Tb_{0.3}Dy_{0.7}Fe_{1.9}$. *J. Appl. Phys.* **1988**, *63*, 3910. [CrossRef]

5.   Humphries, M. *Rare Earth Elements: The Global Supply Chain*; Diane Publishing Company: Collingdale, PA, USA, 2010.

6.   Olabi, A.G.; Grunwald, A. Design and application of magnetostrictive materials. *Mater. Des.* **2008**, *29*, 469–483. [CrossRef]

7.   Kellogg, R.A. Development and Modelling of Iron-Gallium Alloys. Ph.D. Thesis, Iowa State University, Ames, IA, USA, 2003.

8.   Atulasimha, J.; Flatau, A.B. A review of magnetostrictive iron-gallium alloys. *Smart Mater. Struct.* **2011**, *20*, 043001. [CrossRef]

9.   Xing, Q.; Du, Y.; McQueeney, R.J.; Lograsso, T.A. Structural investigations of Fe-Ga alloys: Phase relations and magnetostrictive behavior. *Acta Mater.* **2008**, *56*, 4536–4546. [CrossRef]

10.   Lograsso, T.A.; Summers, E.M. Detection and quantification of $D0_3$ chemical order in Fe-Ga alloys using high resolution X-ray diffraction. *Mater. Sci. Eng. A* **2006**, *416*, 240–245. [CrossRef]

11.   Srisukhumbowornchai, N.; Guruswamy, S. Influence of ordering on the magnetostriction of Fe–27.5 at.% Ga alloys. *J. Appl. Phys.* **2002**, *92*, 5371. [CrossRef]

12.   Taheri, P.; Barua, R.; Hsu, J.; Zamanpour, M.; Chen, Y.; Harris, V.G. Structure, magnetism, and magnetostrictive properties of mechanically alloyed $Fe_{81}Ga_{19}$. *J. Alloys Compd.* **2016**, *661*, 306–311. [CrossRef]

13.   Atulasimha, J.; Flatau, A.B.; Cullen, J.R. Analysis of the effect of gallium content on the magnetomechanical behavior of single-crystal FeGa alloys using an energy-based model. *Smart Mater. Struct.* **2008**, *17*, 025027. [CrossRef]

14.   Hattrick-Simpers, J.R.; Hunter, D.; Craciunescu, C.M.; Jang, K.S.; Murakami, M.; Cullen, J.; Wuttig, M.; Takeuchi, I.; Lofland, S.E.; Bendersky, L.; et al. Combinatorial Investigation of Magnetostriction in FeGa and FeGa-Al. *Appl. Phys. Lett.* **2008**, *93*, 8–13. [CrossRef]

15.   Mungsantisuk, P.; Corson, R.P.; Guruswamy, S. Influence of Be and Al on the magnetostrictive behavior of FeGa alloys. *J. Appl. Phys.* **2005**, *98*, 1–7. [CrossRef]

16.   Dai, L.; Cullen, J.; Wuttig, M.; Lograsso, T.; Quandt, E. Magnetism, elasticity, and magnetostriction of FeCoGa alloys. *J. Appl. Phys.* **2003**, *93*, 8627–8629. [CrossRef]

17.   Restorff, J.B.; Clark, A.E.; Lograsso, T.A.; Ross, A.R. Magnetostriction of ternary Fe-Ga-X alloys (X = Ni, Mo, Sn, Al). *J. Appl. Phys.* **2002**, *91*, 8225. [CrossRef]

18.   Clark, A.E.; Restorff, J.B.; Wunfogle, M.; Hathaway, K.B.; Lograsso, T.A. Magnetostriction of ternary Fe-Ga-X (X = C, V, Cr, Mn, Co, Rh) alloys. *J. Appl. Phys.* **2016**, *507*, 99–102. [CrossRef]

19.   Huang, M.; Lograsso, T.A.; Clark, A.E.; Restorff, J.B.; Wun-Fogle, M. Effect of interstitial additions on magnetostriction in Fe-Ga alloys. *J. Appl. Phys.* **2008**, *103*, 1–4. [CrossRef]

20.   Jiang, L.; Yang, J.; Hao, H.; Zhang, G.; Wu, S.; Chen, Y.; Obi, O.; Fitchorov, T.; Harris, V.G. Giant enhancement in the magnetostrictive effect of FeGa alloys doped with low levels of terbium. *Appl. Phys. Lett.* **2013**, *102*, 222409. [CrossRef]

21.   Jin, T.; Wu, W.; Jiang, C. Improved magnetostriction of Dy-doped $Fe_{83}Ga_{17}$ melt-spun ribbons. *Scr. Mater.* **2014**, *74*, 100–103. [CrossRef]

22.   Yao, Z.; Tian, X.; Jiang, L.; Hao, H.; Zhang, G.; Wu, S. Influences of rare earth element Ce-doping and melt-spinning on microstructure and magnetostriction of $Fe_{83}Ga_{17}$ alloy. *J. Alloys Compd.* **2015**, *637*, 431–435. [CrossRef]

23.   Jiheng, L.I.; Ximing, X.; Chao, Y.; Xuexu, G.A.O.; Xiaoqian, B.A.O. Effect of yttrium on the mechanical and magnetostrictive properties of $Fe_{83}Ga_{17}$ alloy. *J. Rare Earths* **2015**, *33*, 1087–1092.

24.   He, Y.; Jiang, C.; Wu, W.; Wang, B.; Duan, H.; Wang, H.; Zhang, T.; Wang, J.; Liu, J.; Zhang, Z.; et al. Giant heterogeneous magnetostriction in FeGa alloys: Effect of trace element doping. *Acta. Mater.* **2016**, *109*, 177–186. [CrossRef]

25.   Meng, C.; Jiang, C. Magnetostriction of a $Fe_{83}Ga_{17}$ single crystal slightly doped with Tb. *Scr. Mater.* **2016**, *114*, 9–12. [CrossRef]

26. Golovin, I.S.; Balagurov, A.M.; Palacheva, V.V.; Emdadi, A.; Bobrikov, I.A.; Churyumov, A.Y.; Cheverikin, V.V.; Pozdniakov, A.V.; Mikhaylovskaya, A.V.; Golovin, S.A. Influence of Tb on structure and properties of Fe-19% Ga and Fe-27% Ga alloys. *J. Alloys Compd.* **2017**, *707*, 51–56. [CrossRef]

27. Wei, W.; Jiang, C. Improved magnetostriction of Fe$_{83}$Ga$_{17}$ ribbons doped with Sm. *Rare Met.* **2017**, *36*, 18–22.

28. He, Y.; Ke, X.; Jiang, C.; Miao, N.; Wang, H.; Coey, J.M.D.; Wang, Y.; Xu, H. Interaction of Trace Rare-Earth Dopants and Nanoheterogeneities Induces Giant Magnetostriction in Fe-Ga Alloys. *Adv. Funct. Mater.* **2018**, *28*, 1800858. [CrossRef]

29. Novak, G.A.; Colville, A.A. A practical interactive least-squares cell-parameter program using an electronic spreadsheet and a personal computer. *Am. Miner.* **1989**, *74*, 488–490.

30. Koblischka-Veneva, A.; Koblischka, M.R.; Simon, P. Electron backscatter diffraction study of polycrystalline YBa$_2$Cu$_3$O$_{7-\delta}$. *Phys. C: Supercond.* **2002**, *382*, 311–322. [CrossRef]

31. Koblischka-Veneva, A.; Muchlich, F.; Koblischka, M.R.; Babu, N.H.; Cardwell, D.A. Crystallographic Orientation of Y$_2$Ba$_4$CuMO. *J. Am. Ceram. Soc.* **2007**, *90*, 2582–2588. [CrossRef]

32. Chen, Y.; Gillette, S.M.; Fitchorov, T.; Jiang, L.; Hao, H.; Li, J.; Gao, X.; Geiler, A.; Vittoria, C.; Harris, V.G. Quasi-one-dimensional miniature multiferroic magnetic field sensor with high sensitivity at zero bias field. *J. Appl. Phys.* **2011**, *99*, 042505. [CrossRef]

33. Geiler, A.L.; Gillette, S.M.; Chen, Y.; Wang, J.; Chen, Z.; Yoon, S.D.; He, P.; Gao, J.; Vittoria, C.; Harris, V.G. Multiferroic heterostructure fringe field tuning of meander line microstrip ferrite phase shifter. *Appl. Phys. Lett.* **2010**, *96*, 053508. [CrossRef]

34. Fitchorov, T.; Chen, Y.; Hu, B.; Gillette, S.M.; Geiler, A.; Vittoria, C.; Harris, V.G. Tunable fringe magnetic fields induced by converse magnetoelectric coupling in a FeGa/PMN-PT multiferroic heterostructure. *J. Appl. Phys.* **2011**, *110*, 123916. [CrossRef]

35. Stephan, M.; Jahns, R.; Greve, H.; Quandt, E.; Knöchel, R.; Wagner, B. MEMS magnetic field sensor based on magnetoelectric composites. *J. Micromech. Microeng.* **2012**, *22*, 6.

36. Dong, S.; Zhai, J.; Li, J.; Viehland, D.; Summers, E. Strong magnetoelectric charge coupling in stress-biased multilayer-piezoelectric/magnetostrictive composites. *J. Appl. Phys.* **2007**, *101*, 124102. [CrossRef]

37. Clark, A.E.; Hathaway, K.B.; Wun-Fogle, M.; Restorff, J.B.; Lograsso, T.A.; Keppens, V.M.; Petculescu, G.; Taylor, R.A. Extraordinary magnetoelasticity and lattice softening in bcc Fe-Ga alloys. *J. Appl. Phys.* **2003**, *93*, 8621. [CrossRef]

38. Wu, W.; Liu, J.; Jiang, C.; Xu, H. Giant magnetostriction in Tb-doped Fe$_{83}$Ga$_{17}$ melt-spun ribbons. *Appl. Phys. Lett.* **2013**, *103*, 262403. [CrossRef]